


Enhancement of Microorganism Swimming Speed in Active Matter

Harsh Soni,¹ Robert A. Pelcovits,² and Thomas R. Powers^{1,2}

¹*School of Engineering, Brown University, Providence, Rhode Island 02912, USA*

²*Department of Physics, Brown University, Providence, Rhode Island 02012, USA*

 (Received 11 July 2018; published 25 October 2018)

We study a swimming undulating sheet in the isotropic phase of an active nematic liquid crystal. Activity changes the effective shear viscosity, reducing it to zero at a critical value of activity. Expanding in the sheet amplitude, we find that the correction to the swimming speed due to activity is inversely proportional to the effective shear viscosity. Our perturbative calculation becomes invalid near the critical value of activity; using numerical methods to probe this regime, we find that activity enhances the swimming speed by an order of magnitude compared to the passive case.

DOI: 10.1103/PhysRevLett.121.178002

Recent years have seen many advances in the study of swimming at the micron scale in viscous fluids [1], including the creation of artificial microswimmers [2–4], measurements of flows induced by single swimmers [5–7], and the development of hydrodynamic theories [8–10] and simulations [11–13]. The field has expanded to include swimmers in non-Newtonian fluids, such as viscoelastic polymer solutions [14–19] and liquid crystals [20–22]. All of these studies involve passive fluids, in which the energy that drives the flow is added by the internal motors of the swimmer or an external source such as a rotating magnetic field. In active fluids, on the other hand, the energy that drives the flow is added to the system at the level of the microscopic constituents of the fluid [23]. For example, a suspension of molecular motors and cytoskeletal filaments shows spontaneous flows due to the consumption of ATP in the suspension by the molecular motors [24,25]. It is natural to ask if an active fluid can do work on a swimmer, causing it to swim faster than it would in a passive fluid with the same stroke. In this Letter we investigate this question with the Taylor model of a waving sheet [26] in the isotropic phase of an active nematic liquid crystal (Fig. 1).

We use the Taylor sheet because it is one of the simplest models for a flagellated swimmer for which analytical calculations of swimming speed are possible. The isotropic state of the fluid is also chosen for simplicity. Below a critical activity, the undisturbed stable state of the active liquid crystal is isotropic with no flow. The motion of a swimmer induces flows around the swimmer, which in turn lead to local order; the simple nature of the base state allows us to treat the swimmer problem perturbatively. An example of an experimental system with activity and isotropy is the suspension of microtubules, kinesin, and depleting polymers studied by Wu *et al.* [27]. An unconfined active nematic in the nematic phase is unstable to spontaneous flow at any value of activity [28], making an analytic approach difficult.

We model the isotropic phase of an active nematic by adding activity to de Gennes' hydrodynamic model [29–31] for the isotropic phase of a passive nematic. Our work is complementary to but different from a recent study of swimming in an active transversely isotropic medium [32,33], which does not have an entropic force driving the system back to isotropy. Our governing equations are similar to those used in other studies of active matter [34–36]. A striking feature of the active isotropic phase of extensile prolate particles (or contractile oblate particles) is that activity reduces the effective shear viscosity (Fig. 2) [34] and can even cause the apparent shear viscosity to vanish [37–41]. We find that the swimming speed for a small-amplitude Taylor sheet in our active medium is inversely proportional to the effective shear viscosity. Since our perturbative calculation breaks down when the effective shear viscosity gets too small, we use numerical finite-element methods to show that the swimming speed for small effective viscosity can be an order of magnitude larger than the speed in a passive medium for the same stroke. The outline of this Letter is as follows: After introducing the governing equations, we find the critical value of the activity at which the quiescent isotropic state in an infinite domain becomes unstable. Then we calculate the

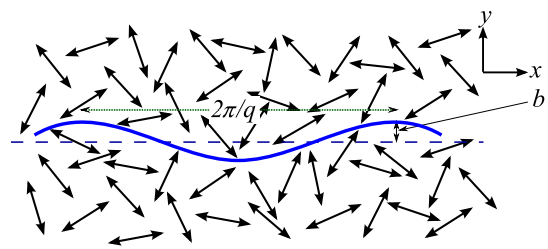


FIG. 1. A Taylor sheet (blue wavy line) with wave number q and amplitude b swimming in an active nematic fluid (double-headed arrows) in the isotropic phase.

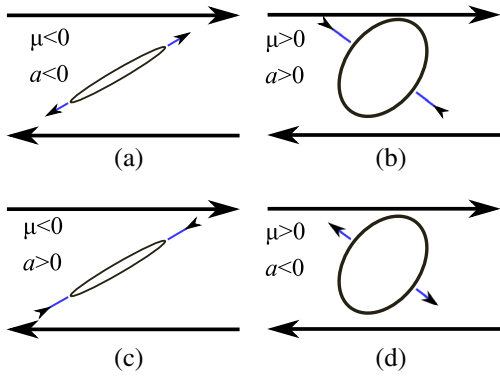


FIG. 2. Effect of activity a on the effective shear viscosity. The large arrows represent the flow, and the small arrows represent the active forces. (a) Extensile prolate particles and (b) contractile oblate particles reduce the shear viscosity [34]. The force axis is assumed along the particle axis of symmetry. (c) Contractile prolate particles and (d) extensile oblate particles increase the shear viscosity [34].

swimming speed using perturbation theory, which is valid when the activity is sufficiently smaller than the critical value for instability. Finally, we numerically calculate the flow, order parameter field, and swimming speed, again assuming that the activity is less than the critical value.

To motivate the governing equations, we begin with the nematic degrees of freedom. For simplicity, we suppose there is no variation in the spatial direction perpendicular to the x - y plane (Fig. 1). Thus, the local nematic ordering is characterized by a symmetric traceless order parameter tensor $Q_{\alpha\beta}$, with $\alpha, \beta = x, y$. To leading order in $Q_{\alpha\beta}$, the Landau–de Gennes free energy density is [30]

$$\mathcal{F} = \frac{A}{2} Q_{\alpha\beta} Q_{\alpha\beta}, \quad (1)$$

where we sum over repeated indices and $A > 0$ in the isotropic phase. Frank elasticity can be neglected in the isotropic phase, as can higher-order terms in $Q_{\alpha\beta}$ (note that a cubic term is identically zero in two dimensions). We also disregard a quartic term, which plays little role in our expansion about the isotropic state, but would be required to limit the amplitude of the order parameter when the isotropic state is unstable. Thus, the molecular field is $\Phi_{\alpha\beta} \equiv -\partial\mathcal{F}/\partial Q_{\alpha\beta} = -A Q_{\alpha\beta}$ in the isotropic phase. The equilibrium stress is the Ericksen stress, $\sigma_{\alpha\beta}^e = \mathcal{F}\delta_{\alpha\beta} - \partial\mathcal{F}/\partial(\partial_\beta Q_{\mu\nu})\partial_\alpha Q_{\mu\nu}$ [29,42].

The rate of entropy production per volume is [30]

$$T\dot{S} = \sigma'_{\alpha\beta} e_{\alpha\beta} + \Phi_{\alpha\beta} R_{\alpha\beta}, \quad (2)$$

where T is temperature, S is entropy per volume, $\sigma'_{\alpha\beta}$ is the viscous stress tensor, $e_{\alpha\beta} = (\partial_\alpha v_\beta + \partial_\beta v_\alpha)/2$ is the strain rate tensor, v_α is the velocity field, and $R_{\alpha\beta}$ is the rate of change of $Q_{\alpha\beta}$ relative to the local rate of rotation $\omega_{\alpha\beta} = (\partial_\alpha v_\beta - \partial_\beta v_\alpha)/2$ of the background fluid,

$R_{\alpha\beta} = \partial_t Q_{\alpha\beta} + \mathbf{v} \cdot \nabla Q_{\alpha\beta} + \omega_{\alpha\gamma} Q_{\gamma\beta} - Q_{\alpha\gamma} \omega_{\gamma\beta}$. Following de Gennes [29], we take the forces in the entropy source to be the molecular field $\Phi_{\alpha\beta}$ and the viscous stress tensor $\sigma'_{\alpha\beta}$, and the corresponding fluxes to be $e_{\alpha\beta}$ and $R_{\alpha\beta}$. Assuming that the forces are linear functions of the fluxes, the phenomenological equations relating the forces to the fluxes are

$$\sigma'_{\alpha\beta} = 2\eta e_{\alpha\beta} + 2(\mu + \mu_1)R_{\alpha\beta} + aQ_{\alpha\beta}, \quad (3)$$

$$\Phi_{\alpha\beta} = 2\mu e_{\alpha\beta} + \nu R_{\alpha\beta}, \quad (4)$$

where η is the shear viscosity, μ and μ_1 couple shear and alignment, and ν is the rotational viscosity. We neglect higher-order terms such as $Q_{\alpha\gamma} e_{\gamma\delta} Q_{\delta\beta}$, since the magnitude of the order parameter is small in the isotropic phase; again, such terms should be retained when the order parameter is nonvanishing [36]. The coefficients μ_1 and a arise from activity. When $a = 0$ and $\mu_1 = 0$, the Onsager reciprocal relations [43] hold, and the rate of entropy production is positive, implying $\eta\nu - 2\mu^2 > 0$. Thus, the active parameter μ_1 determines the degree of violation of the Onsager relations, and, when it is sufficiently positive, can lead to a negative rate of entropy production.

The active stress is $aQ_{\alpha\beta}$ [34], with $a < 0$ for extensile particles and $a > 0$ for contractile particles. The coupling μ controls the orientation of the particles in shear flow, leading to shear birefringence. For example, nematic order develops in a weak steady shear flow, with $Q_{\alpha\beta} = -(2\mu/A)e_{\alpha\beta}$ to first order in the strain rate [29]. Independent of the value of μ_1 , particles align their symmetry axes with one of the principal axes of the shear, with prolate particles ($\mu < 0$) and oblate particles ($\mu > 0$) aligning along different axes (Fig. 2).

The governing equations are the director equation (4) and the force balance equation $\partial_\beta \sigma_{\alpha\beta} = 0$, with $\sigma_{\alpha\beta} = -p\delta_{\alpha\beta} + \sigma_{\alpha\beta}^e + \sigma'_{\alpha\beta}$. We define the effective viscosity η_{eff} and the effective coupling μ_{eff} by using Eq. (4) to eliminate $Q_{\alpha\beta}$ from the stress, Eq. (3), to find $\sigma'_{\alpha\beta} = 2\eta_{\text{eff}}e_{\alpha\beta} + 2\mu_{\text{eff}}R_{\alpha\beta}$, where $\eta_{\text{eff}} = \eta - \mu a/A$ and $\mu_{\text{eff}} = \mu + \mu_1 - \nu a/(2A)$. Thus, activity gives rise to an effective shear viscosity η_{eff} , which vanishes at a critical value of the activity $a_c = A\eta/\mu$.

Next, we turn to the linear stability analysis of the state with $v_\alpha = 0$ and $Q_{\alpha\beta} = 0$, in an infinite unbounded domain. To linear order, the force balance equation is $-\partial_\alpha p + 2\eta_{\text{eff}}\partial_\beta e_{\alpha\beta} + 2\mu_{\text{eff}}\partial_\beta \partial_t Q_{\alpha\beta} = 0$. The pressure p is determined by the incompressibility constraint, $\partial_\alpha v_\alpha = 0$. It is convenient to enforce incompressibility with the stream function ψ , defined so that $\mathbf{v} = \nabla \times \psi \hat{\mathbf{z}}$. Also, in two dimensions, the tensor-order parameter $Q_{\alpha\beta}$ is related to the scalar-order parameter S and the director \mathbf{n} via $Q_{\alpha\beta} = S(2n_\alpha n_\beta - \delta_{\alpha\beta})$. The linearized equations for the stream function and the order parameter are

$$\Delta^2 \psi - 2 \frac{\mu_{\text{eff}}}{\eta_{\text{eff}}} [(\partial_x^2 - \partial_y^2) \partial_t Q_{xy} - 2 \partial_x \partial_y \partial_t Q_{xx}] = 0, \quad (5)$$

$$2\mu \partial_x \partial_y \psi + A Q_{xx} + \nu \partial_t Q_{xx} = 0, \quad (6)$$

$$-\mu(\partial_x^2 - \partial_y^2) \psi + A Q_{xy} + \nu \partial_t Q_{xy} = 0, \quad (7)$$

where $\Delta = \partial_x^2 + \partial_y^2$.

For perturbations of the velocity and order-parameter tensor proportional to $\exp(i\mathbf{q} \cdot \mathbf{x} + \sigma t)$, the characteristic equation for this problem yields two roots (see the Supplemental Material [44]):

$$\sigma_1 = -A/\nu, \quad (8)$$

$$\sigma_2 = -A\eta_{\text{eff}}/(\eta_{\text{eff}}\nu - 2\mu\mu_{\text{eff}}). \quad (9)$$

The first root σ_1 is always negative; inserting $\exp(i\mathbf{q} \cdot \mathbf{x} + \sigma_1 t)$ into Eq. (6) or Eq. (7) reveals that this mode has no flow, with the director \mathbf{n} always parallel to \mathbf{q} , and the scalar-order parameter relaxing to zero with rate A/ν .

The second root corresponds to a mode in which there is a shear flow with a velocity perpendicular to \mathbf{q} (due to incompressibility $\mathbf{q} \cdot \mathbf{v} = 0$), with \mathbf{n} at 45° to the flow. The numerator in Eq. (9) is precisely the quantity that determines whether or not the entropy production $T\dot{S}$ is positive. If μ_1 is small enough that $\eta_{\text{eff}}\nu - 2\mu\mu_{\text{eff}} > 0$, then the isotropic state is unstable when $\eta_{\text{eff}} < 0$; i.e., $a > a_c = A\eta/\mu$ for positive μ [Fig. 2(b)], or $a < a_c = A\eta/\mu$ for negative μ [Fig. 2(a)]. The quiescent isotropic state is unstable against shear flow and local ordering when the shear-induced orientation of the particles leads to greater shear flow, as in Figs. 2(a) and 2(b).

We now consider a Taylor swimmer with $y = h(x, t) \equiv b \cos(qx - \omega t)$ (Fig. 1) in the stable phase of an isotropic active nematic. Our approach is the same as Lauga's calculation for a dilute polymer solution [14]. To calculate the swimming speed of the sheet, we work in the rest frame of the swimmer and solve the governing Eqs. (3) and (4) with no-slip boundary conditions on the velocity at the swimmer, $\mathbf{v}(x, y = h) = \partial_t h(x, t) \hat{\mathbf{y}}$. The unknown velocity at $y \rightarrow \infty$ is the negative of the swimming velocity U . No boundary conditions are imposed on the order parameter, because we have disregarded the Frank energy. We assume that $\epsilon = bq \ll 1$ and expand in powers of ϵ , so that, e.g., $\psi = \epsilon\psi^{(1)} + \epsilon^2\psi^{(2)}$. To first order in ϵ , the Eqs. (5)–(7) yield

$$\begin{aligned} \psi^{(1)} &= (\omega/q^2)(1 + qy)e^{-qy} \cos(qx - \omega t), \\ Q_{xx}^{(1)} &= \frac{-2qy\omega\mu e^{-qy}}{A^2 + \omega^2\nu^2} [\omega\nu \cos(qx - \omega t) + A \sin(qx - \omega t)], \\ Q_{xy}^{(1)} &= \frac{-2qy\omega\mu e^{-qy}}{A^2 + \omega^2\nu^2} [A \cos(qx - \omega t) - \omega\nu \sin(qx - \omega t)]. \end{aligned} \quad (10)$$

The velocity field is the same as the Stokes flow found by Taylor [26] for a Newtonian fluid, and the order parameter is independent of the activity. Note that the direction of \mathbf{n} is independent of y to first order in ϵ , since the ratio $Q_{xy}^{(1)}/Q_{xx}^{(1)}$ is independent of y .

The power P_s supplied by the swimmer is equal to the sum of the rate of change of the free energy and the net power dissipated in the fluid, $P_s = dF/dt + P_f$, where $F = \int d^3x \mathcal{F}$ and

$$P_s = \int \left(v_\alpha \sigma_{\alpha\beta} + \frac{\partial \mathcal{F}}{\partial (\partial_\beta Q_{\mu\nu})} \frac{dQ_{\mu\nu}}{dt} \right) N_\beta dS, \quad (11)$$

$$P_f = \int \left(e_{\alpha\beta} (\sigma_{\alpha\beta} - \sigma_{\alpha\beta}^e) + \Phi_{\alpha\beta} \frac{dQ_{\alpha\beta}}{dt} \right) d^3x. \quad (12)$$

Here $dQ_{\alpha\beta}/dt = \partial_t Q_{\alpha\beta} + v_\gamma \partial_\gamma Q_{\alpha\beta}$, dS is the area element of the swimmer, and $\hat{\mathbf{N}}$ is the downward-pointing normal to the swimmer. Note that the net power dissipated in the fluid may be negative due to activity. The first-order solutions allow us to calculate the leading-order rate of working of the swimmer per unit area of the sheet,

$$\mathcal{P}_s \approx b^2 q \omega^2 \left[\eta_{\text{eff}} - \frac{2\nu\mu\mu_{\text{eff}}\omega^2}{A^2 + \nu^2\omega^2} \right] \quad (13)$$

(note that $P_s = \int dS \mathcal{P}_s$). The power supplied by the swimmer decreases linearly with activity a (Fig. 3, green solid line). The fluid does net positive work on the swimmer when $a > a_0 = a_c + [\eta\nu - 2\mu(\mu + \mu_1)]\omega^2/(A\mu)$. The value of a_0 can be less than a_c and in the regime where our perturbative calculation is valid when μ_1 is sufficiently

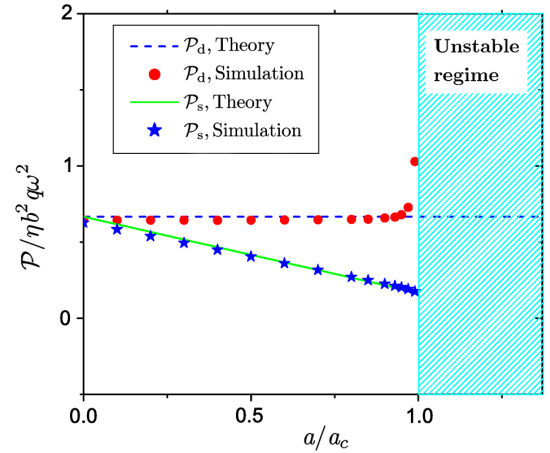


FIG. 3. Dimensionless rate of work \mathcal{P}_s of the swimmer [green solid line from theory, Eq. (13), blue stars from simulations] vs dimensionless activity a/a_c ; and dimensionless rate of dissipation of energy \mathcal{P}_d (blue dashed line from theory, red dots from simulation) vs dimensionless activity a/a_c , for $\epsilon = bq = 0.1$, $\mu = \eta = \nu/3$, $A = \nu\omega$, and $\mu_1 = 0$.

large and positive. We denote the power dissipated in the fluid per unit area of the sheet by $\mathcal{P}_d = \int [e_{\alpha\beta}(2\eta e_{\alpha\beta} + 2\mu R_{\alpha\beta}) + \Phi_{\alpha\beta} dQ_{\alpha\beta}/dt] d^3x / \int dS$. To leading order, \mathcal{P}_d is positive and independent of activity (Fig. 3, blue dashed line), and is given by Eq. (13) with η_{eff} replaced by η and μ_{eff} replaced by μ . Near the critical activity, nonlinear effects become important, and \mathcal{P}_d depends on a , since the dependence of \mathbf{v} and Φ on a becomes discernible (Fig. 3, red dots).

To find the swimming speed, it is convenient to write the time average of the x component of momentum balance in terms of the velocity and expand to $\mathcal{O}(\epsilon^2)$:

$$\eta_{\text{eff}} \frac{d^2}{dy^2} \langle v_x^{(2)} \rangle + 4e^{-2qy} (qy - 2) y q^2 \omega^3 \frac{2\mu\nu\mu_{\text{eff}}}{A^2 + \nu^2\omega^2} = 0. \quad (14)$$

Enforcing the no-slip boundary condition to second order leads to $\langle v_x^{(2)}(x, 0) \rangle = \omega/(2q)$. Solving for the flow leads to the swimming speed

$$U = \frac{c\epsilon^2}{2} \left[1 - \frac{2\nu\mu\mu_{\text{eff}}\omega^2}{\eta_{\text{eff}}(A^2 + \nu^2\omega^2)} \right], \quad (15)$$

where $c = \omega/q$ is the wave speed of the deformation of the swimmer, and we are using the convention that a positive U means the swimmer moves left in the laboratory frame. In the Supplemental Material [44], we show that the swimming speed of a two-dimensional squirmer has a similar dependence on the material parameters ν , μ , μ_{eff} , η_{eff} , and A . The swimming speed diverges when $a \rightarrow a_c$, since the effective shear viscosity vanishes at the critical activity, indicating a breakdown of the perturbative calculation. Analyzing the form of the next-order terms reveals that they are of the order of $\epsilon^4/(a_c - a)^3$, indicating that the perturbative approach requires $\epsilon^2 \ll (a_c - a)^2$. Also, when $a < a_c$, U is positive. Thus, as long as the fluid is stable, activity cannot make the swimmer swim in the direction of the propagating waves.

To go beyond the restriction $\epsilon^2 \ll (a_c - a)^2$, we solve the force balance equation $\partial_\beta \sigma_{\alpha\beta} = 0$ and the director equation (4) numerically using the COMSOL Multiphysics software [46]. We scale length by $1/q$ and time by $1/\omega$, and we choose $\epsilon = 0.1$, $\mu = \eta = \nu/3$, $A = \nu\omega$, and $\mu_1 = 0$. To approximate the infinite system, we choose a size for the simulation box much larger than the decay length $1/q$. The simulation box has dimensions 32π and 60 along the x and y directions, respectively, with periodic boundary conditions along the x direction. The Taylor sheet is represented by the top wall (see Fig. 2 of the Supplemental Material [44]), which deforms and has a no-slip boundary condition. In order to ensure that the sheet is subjected to no net force along the x direction, we choose the slip boundary condition $\sigma_{xy} = 0$ on the bottom wall. More details of the

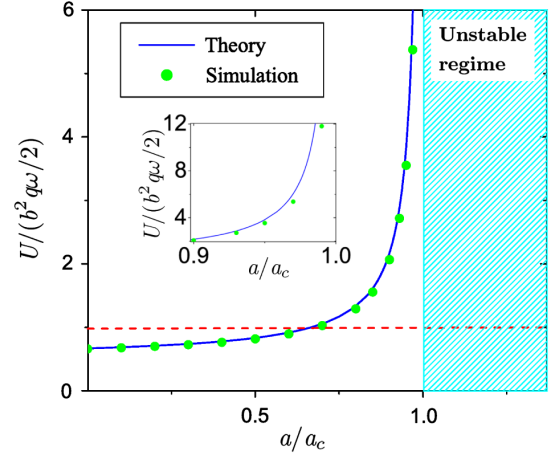


FIG. 4. Dimensionless swimming speed vs dimensionless activity from theory [Eq. (15)] (blue line) and simulations (green dots). The parameters used are the same as in Fig. 3. The inset shows the critical region $a \approx a_c$.

numerical method are discussed in the Supplemental Material [44].

Figure 4 shows the numerically calculated U vs a for $a < a_c$. The speed U increases with a monotonically, with good agreement between the simulations and theory when $a < 0.9a_c$. At $a = 0.99a_c$, U is enhanced up to around 12 times the swimming speed of the Taylor case (see the inset of Fig. 4). We do not perform numerical studies much closer to the critical activity because the decay length increases as $a \rightarrow a_c$, requiring a larger simulation box. Note that a robust feature of our result is that although we have chosen $A = \nu\omega$ for Fig. 4, the sharp rise in swimming speed only relies on the vanishing of η_{eff} at $a = a_c$. In Fig. 2 of the Supplemental Material [44], we show the flow profile around the Taylor sheet superposed with a heat map of the nematic order parameter. The latter attains its greatest values in the regions where the shear is greatest.

The numerically calculated power exerted by the swimmer and the power dissipated in the fluid are shown in Fig. 3. The power exerted by the swimmer decreases with increasing activity (blue stars), whereas the rate of dissipation increases with increasing activity (red dots). When $a = 0$, the power exerted by the swimmer equals the power dissipated in the fluid. However, in the presence of activity, the swimmer does not work as hard, since part of the power generated by activity contributes to work on the swimmer, and part is dissipated in the fluid.

We have studied the swimming of a model microorganism in the isotropic phase of an active nematic liquid crystal. It would be natural to look for the predicted increase in swimming speed in an isotropic active microtubule system [27]. We found that the waving sheet and the squirmer both have a similar dependence of speed on activity, and that the sharp increase in speed with activity only requires the speed to depend inversely on the effective shear viscosity. Thus, we

expect that the increase is robust against changes in the swimming mechanism, and that the increase could be seen in experiments with undulatory swimmers such as *Caenorhabditis elegans* [17] or synthetic microswimmers such as rotating helices [47]. An important extension of this work would be to study a swimmer in *polar* active matter, such as *C. elegans* in a suspension of *Escherichia coli* bacteria [48]. It would also be interesting to generalize our work to the unsteady regime above the critical activity.

We thank Aparna Baskaran, Ray Goldstein, David Henann, Oleg Lavrentovich, and Sriram Ramaswamy for helpful discussions. This work was supported in part by National Science Foundation Grant No. CBET-1437195 and National Science Foundation Grant No. MRSEC-1420382.

-
- [1] E. Lauga and T. R. Powers, *Rep. Prog. Phys.* **72**, 096601 (2009).
- [2] K. Ishiyama, M. Sendoh, A. Yamazaki, and K. I. Aral, *Sens. Actuators A* **91**, 141 (2001).
- [3] R. Dreyfus, J. Baudry, M. L. Roper, M. Fermigier, H. A. Stone, and J. Bibette, *Nature (London)* **437**, 862 (2005).
- [4] A. Ghosh and P. Fischer, *Nano Lett.* **9**, 2243 (2009).
- [5] J. S. Guasto, K. A. Johnson, and J. P. Gollub, *Phys. Rev. Lett.* **105**, 168102 (2010).
- [6] K. Drescher, J. Dunkel, L. H. Cisneros, S. Ganguly, and R. E. Goldstein, *Proc. Natl. Acad. Sci. U.S.A.* **108**, 10940 (2011).
- [7] R. E. Goldstein, *Annu. Rev. Fluid Mech.* **47**, 343 (2015).
- [8] H. A. Stone and A. D. T. Samuel, *Phys. Rev. Lett.* **77**, 4102 (1996).
- [9] A. Najafi and R. Golestanian, *J. Phys. Condens. Matter* **17**, S1203 (2005).
- [10] O. S. Pak and E. Lauga, in *Low-Reynolds-Number Flows: Fluid-Structure Interactions*, RSC Soft Matter Series Vol. 4, edited by E. Duprat and H. A. Stone (Royal Society of Chemistry, Cambridge, 2015) p. 100.
- [11] C. Pozrikidis, *Boundary Integral and Singularity Methods for Linearized Viscous Flow* (Cambridge University Press, Cambridge, 1992).
- [12] S. Cortez, *SIAM J. Sci. Comput.* **23**, 1204 (2001).
- [13] R. Cortez, L. Fauci, and A. Medovikov, *Phys. Fluids* **17**, 031504 (2005).
- [14] E. Lauga, *Phys. Fluids* **19**, 083104 (2007).
- [15] H. C. Fu, T. R. Powers, and C. W. Wolgemuth, *Phys. Rev. Lett.* **99**, 258101 (2007).
- [16] J. Teran, L. Fauci, and M. Shelley, *Phys. Rev. Lett.* **104**, 038101 (2010).
- [17] X. N. Shen and P. E. Arratia, *Phys. Rev. Lett.* **106**, 208101 (2011).
- [18] B. Liu, T. R. Powers, and K. S. Breuer, *Proc. Natl. Acad. Sci. U.S.A.* **108**, 19516 (2011).
- [19] *Complex Fluids in Biological Systems*, edited by S. E. Spagnolie (Springer, New York, 2015).
- [20] S. Zhou, A. Sokolov, O. D. Lavrentovich, and I. S. Aranson, *Proc. Natl. Acad. Sci. U.S.A.* **111**, 1265 (2014).
- [21] P. C. Mushenheim, R. R. Trivedi, H. H. Tuson, D. B. Weibel, and N. L. Abbott, *Soft Matter* **10**, 88 (2014).
- [22] M. S. Krieger, S. E. Spagnolie, and T. R. Powers, *Phys. Rev. E* **90**, 052503 (2014).
- [23] M. C. Marchetti, J. F. Joanny, S. Ramaswamy, T. B. Liverpool, J. Prost, M. Rao, and R. A. Simha, *Rev. Mod. Phys.* **85**, 1143 (2013).
- [24] V. Schaller, C. Weber, C. Semmrich, E. Frey, and A. R. Bausch, *Nature (London)* **467**, 73 (2010).
- [25] T. Sanchez, D. T. N. Chen, S. J. DeCamp, M. Heymann, and Z. Dogic, *Nature (London)* **491**, 431 (2012).
- [26] G. Taylor, *Proc. R. Soc. A* **209**, 447 (1951).
- [27] K.-T. Wu, J. B. Hishamunda, D. T. N. Chen, S. J. DeCamp, Y.-W. Chang, A. Fernández-Nieves, S. Fraden, and Z. Dogic, *Science* **355**, eaal1979 (2017).
- [28] L. Giomi, L. Mahadevan, B. Chakraborty, and M. F. Hagan, *Nonlinearity* **25**, 2245 (2012).
- [29] P. G. de Gennes, *Phys. Lett. A* **30**, 454 (1969).
- [30] P. G. de Gennes and J. Prost, *The Physics of Liquid Crystals* (Clarendon Press/Oxford University Press, Oxford/New York, 1993).
- [31] P. G. de Gennes, *Mol. Cryst. Liq. Cryst.* **12**, 193 (1971).
- [32] G. Cupples, R. J. Dyson, and D. J. Smith, *J. Fluid Mech.* **812**, 501 (2017).
- [33] G. Cupples, R. J. Dyson, and D. J. Smith, *J. Fluid Mech.* **855**, 408 (2018).
- [34] Y. Hatwalne, S. Ramaswamy, M. Rao, and R. A. Simha, *Phys. Rev. Lett.* **92**, 118101 (2004).
- [35] D. Saintillan and M. J. Shelley, *Phys. Rev. Lett.* **100**, 178103 (2008).
- [36] F. G. Woodhouse and R. E. Goldstein, *Phys. Rev. Lett.* **109**, 168105 (2012).
- [37] M. E. Cates, S. M. Fielding, D. Marenduzzo, E. Orlandini, and J. M. Yeomans, *Phys. Rev. Lett.* **101**, 068102 (2008).
- [38] A. Sokolov and I. S. Aranson, *Phys. Rev. Lett.* **103**, 148101 (2009).
- [39] L. Giomi, T. B. Liverpool, and M. C. Marchetti, *Phys. Rev. E* **81**, 051908 (2010).
- [40] J. Gachelin, G. Miño, H. Berthet, A. Lindner, A. Rousselet, and E. Clément, *Phys. Rev. Lett.* **110**, 268103 (2013).
- [41] H. M. López, J. Gachelin, C. Douarache, H. Auradou, and E. Clément, *Phys. Rev. Lett.* **115**, 028301 (2015).
- [42] F. Jülicher, S. W. Grill, and G. Salbreux, *Rep. Prog. Phys.* **81**, 076601 (2018).
- [43] L. Onsager, *Phys. Rev.* **37**, 405 (1931).
- [44] See Supplemental Material at <http://link.aps.org/supplemental/10.1103/PhysRevLett.121.178002> for details of the stability analysis and numerical simulation, calculations of the squirmer swimming speed and next order term in the swimming speed of the sheet, which includes Ref. [45].
- [45] J. R. Blake, *J. Fluid Mech.* **46**, 199 (1971).
- [46] COMSOL, Multiphysics v. 5.2, COMSOL AB, Stockholm, Sweden, www.comsol.com.
- [47] S. Gomez, F. A. Godinez, E. Lauga, and R. Zenit, *J. Fluid Mech.* **812**, R3 (2017).
- [48] S. Thutupalli, S. Uppaluri, G. W. A. Constable, S. A. Levin, H. A. Stone, C. E. Tarnita, and C. P. Brangwynne, *Proc. Natl. Acad. Sci. U.S.A.* **114**, 2289 (2017).